

# Identification of PP1c-PPP1R12A Substrates Using Kinase-Catalyzed Biotinylation to Identify Phosphatase Substrates

Pavithra M. Dedigama-Arachchige, Nuwan P.N. Acharige, Xiangmin Zhang, Hannah J. Bremer, Zhengping Yi, and Mary Kay H. Pflum\*



Cite This: *ACS Omega* 2023, 8, 35628–35637



Read Online

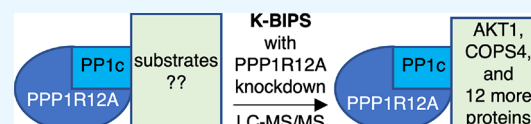
ACCESS |

Metrics & More

Article Recommendations

Supporting Information

**ABSTRACT:** Protein phosphatase 1 regulatory subunit 12A (PPP1R12A) interacts with the catalytic subunit of protein phosphatase 1 (PP1c) to form the myosin phosphatase complex. In addition to a well-documented role in muscle contraction, the PP1c-PPP1R12A complex is associated with cytoskeleton organization, cell migration and adhesion, and insulin signaling. Despite the variety of biological functions, only a few substrates of the PP1c-PPP1R12A complex are characterized, which limit a full understanding of PP1c-PPP1R12A activities in muscle contraction and cytoskeleton regulation. Here, the chemoproteomics method Kinase-catalyzed Biotinylation to Identify Phosphatase Substrates (K-BIPS) was used to identify substrates of the PP1c-PPP1R12A complex in L6 skeletal muscle cells. K-BIPS enriched 136 candidate substrates with 14 high confidence hits. One high confidence hit, AKT1 kinase, was validated as a novel PP1c-PPP1R12A substrate. Given the previously documented role of AKT1 in PPP1R12A phosphorylation and cytoskeleton organization, the data suggest that PP1c-PPP1R12A regulates its own phosphatase activity through an AKT1-dependent feedback mechanism to influence cytoskeletal arrangement in muscle cells.



## INTRODUCTION

Protein phosphorylation, regulated by the activities of protein kinases and phosphatases (Figure 1A), is a ubiquitous post-translational modification in cell biology that profoundly influences protein activity and physical interactions.<sup>1,2</sup> Because of the pivotal role phosphorylation plays in cell biology, kinases are widely studied and are the targets of many pharmaceutical drugs.<sup>3,4</sup> In contrast, research on phosphatases has lagged behind, with fewer well-characterized substrates and mechanisms of action. The slow progress to characterize phosphatase biology is partly explained by their structural complexity.<sup>5</sup> Protein Tyr phosphatases (PTPs) dephosphorylate phosphorylated Tyr residues and carry both catalytic and regulatory subunits on a single protein, which have made them amenable to rigorous study.<sup>6,7</sup> In contrast, many Ser/Thr phosphatases, which act on phosphorylated Ser/Thr substrates, consist of a catalytic subunit protein and a separate regulatory subunit protein that assemble into distinct phosphatase complexes with different substrate preferences.<sup>8,9</sup> Because of the wide variety of regulatory subunits available to Ser/Thr phosphatases, the thorough characterization of each phosphatase-regulatory complex has been challenging, particularly in terms of substrate characterization.

As an important example, Ser/Thr protein phosphatase 1 (PP1) is abundant; is involved in various disease states, including cancer; and can associate with roughly 100 different regulatory subunits.<sup>10</sup> Among these, the regulatory protein subunit PPP1R12A (protein phosphatase 1 regulatory subunit 12A, also known as myosin phosphatase targeting subunit 1 or MYPT1) interacts with PP1c to trigger muscle relaxation in

smooth muscle cells by dephosphorylating myosin regulatory light chain 20 (MLC20).<sup>11,12</sup> Additionally, the PP1c-PPP1R12A complex dephosphorylates merlin,<sup>13</sup> retinoblastoma protein,<sup>14</sup> and PLK1.<sup>15</sup> Beyond these known substrates, PP1c-PPP1R12A is speculated to dephosphorylate other substrates with roles in cytoskeleton organization, cell migration, adhesion, and cell division, in addition to disease states such as cancer and insulin resistance.<sup>16–20</sup> In particular, PP1c-PPP1R12A interacts with insulin receptor substrate 1 (IRS1),<sup>21</sup> and insulin stimulation modulates the phosphorylation of PPP1R12A,<sup>22</sup> which suggests that PP1c-PPP1R12A likely plays a role in insulin signaling. To further study the role of PP1c-PPP1R12A in skeletal muscle insulin signaling, we previously analyzed the phosphoproteome of L6 myoblast cells after inducible PPP1R12A knockdown and titanium dioxide phosphopeptide enrichment as a function of insulin stimulation. Comparing knockdown and uninduced samples, 295 possible protein substrates were observed in either the presence or absence of insulin.<sup>23</sup> Many observed proteins were associated with the mTOR and Rho signaling pathways, which are related to insulin signaling. The proteomics study provided further evidence that the PP1c-PPP1R12A complex plays a role in insulin signaling.

**Received:** March 22, 2023

**Accepted:** July 21, 2023

**Published:** September 21, 2023



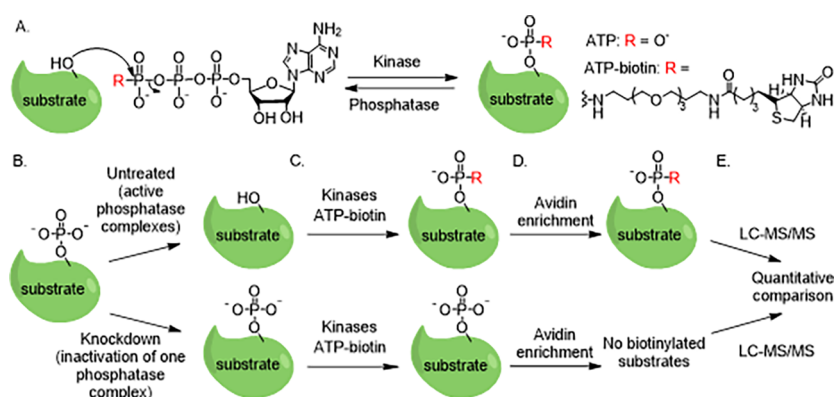


**Figure 1.** Protein phosphorylation and the K-BIPS procedure. (A) Protein kinases transfer a phosphoryl group from adenosine 5'-triphosphate (ATP) to substrate proteins. Protein phosphatases remove the phosphoryl group. With kinase-catalyzed labeling,  $\gamma$ -modified ATP analogs, such as ATP-biotin, are accepted by kinases to modify proteins. (B–E) The K-BIPS method: Untreated lysates (B, top) containing active phosphatase complexes, including PP1c-PPP1R12A, will dephosphorylate substrates to facilitate biotinylation (C). In contrast, knockdown of a regulatory subunit, such as PPP1R12A (B, bottom), blocks the ability for PP1c-PPP1R12A substrates to be biotinylated by ATP-biotin and kinases (C). Following avidin purification (D) and LC-MS/MS analysis (E), proteins enriched in untreated samples compared to inactivated samples are candidate substrates.

To complement the earlier phosphoproteomics analysis, here we applied the chemoproteomics method Kinase-catalyzed Biotinylation to Identify Phosphatase Substrates (K-BIPS)<sup>24</sup> to identify substrates of the PP1c-PPP1R12A complex. K-BIPS exploits the fact that kinases accept the  $\gamma$ -modified ATP analog, ATP-biotin, to biotinylate substrate proteins (Figure 1A).<sup>25–27</sup> One advantage of using kinase-catalyzed biotinylation with ATP-biotin is the focus on dynamically phosphorylated proteins, which avoids non-dynamic phosphoproteins that could suppress identification of low-abundance proteins. Importantly for K-BIPS, kinase-catalyzed biotinylation with ATP-biotin is inefficient without phosphatase activity; active phosphatases are needed to dephosphorylate previously phosphorylated proteins prior to biotinylation by ATP-biotin and endogenous kinases (Figure 1B, top panel).<sup>28</sup> Given the phosphatase dependence, ATP-biotin labeling was carried out in the presence or absence of phosphatase activity (Figure 1B), which resulted in protein biotinylation only in the presence of active phosphatases (Figure 1B, top panel). Because substrates remained unlabeled without active phosphatases (Figure 1B, bottom panel), subsequent enrichment of biotinylated proteins (Figure 1D) and analysis by liquid chromatography–tandem mass spectrometry (LC-MS/MS) and label-free quantitation (Figure 1E) revealed biotinylated phosphatase substrates. Prior work used small molecule inhibitors and knockdown to inactivate phosphatases for K-BIPS, resulting in the identification of multiple substrates of PP1-Gadd34 and PTP1B.<sup>24,29</sup>

To complement prior work, the goal of this study was to use K-BIPS to identify substrates of the PP1c-PPP1R12A phosphatase complex. Moreover, this study used an inducible knockdown system to inactivate phosphatase activity for K-BIPS, which complements prior studies using inhibitor inactivation or knockdown via transient transfection.<sup>24,29</sup> Using K-BIPS with PPP1R12A inducible knockdown in L6 myoblast cells, 136 candidate substrates and 14 high confidence hits were identified. The hit list included proteins with known direct or indirect interactions with the PP1c-PPP1R12A complex, as well as functions in cellular processes associated with PP1c-PPP1R12A in muscle cells, including cytoskeletal organization, cell adhesion, and cell division. Two

high confidence hit proteins, AKT1 and COPS4, were confirmed as K-BIPS hits using western blotting analysis. AKT1 was further validated as a PP1c-PPP1R12A substrate. Combined with earlier work documenting a role of AKT1 and COPS4 in regulating PP1c-PPP1R12A phosphatase activity, the K-BIPS data suggest feedback mechanisms involving AKT1 and COPS4 that contribute to regulate phosphatase activity in muscle cells.

## EXPERIMENTAL SECTION

**Synthesis of ATP-Biotin.** ATP-biotin was synthesized as previously reported.<sup>25</sup>

**Cell Culture and Lysis.** L6 muscle cells ( $20 \times 10^6$ ) stably transduced with lentivirus encoding doxycycline (Dox)-inducible shRNA targeting PPP1R12A<sup>23</sup> were grown in DMEM (45 mL, ThermoFisher) containing 10% FBS (fetal bovine serum, ThermoFisher) and  $1 \times$  antimycotic–antibiotic solution (ThermoFisher) at 37 °C in a 5% CO<sub>2</sub> environment. At ~80% confluency, cells were treated either with doxycycline (Dox, 45  $\mu$ L, 100  $\mu$ g/mL dissolved in DMEM without FBS and antibiotic, Sigma Aldrich, D9891) or vehicle (45  $\mu$ L, DMEM without FBS and antibiotic). Two days later, the medium was removed, and fresh medium containing Dox (45  $\mu$ L, 100  $\mu$ g/mL dissolved in the same DMEM without FBS and antibiotic) or vehicle (45  $\mu$ L, DMEM without FBS and antibiotic) was added. After 16 additional hours, cells were serum-starved with FBS-free DMEM with or without Dox, as described above, containing 0.1% BSA (bovine serum albumin, GenDEPOT, catalog number A0100-010) at 37 °C for 4 h. Serum-starved cells were harvested by adding trypsin-EDTA (0.25%, 12 mL, ThermoFisher) after removing the medium and washing with DPBS (Dulbecco's phosphate-buffered saline, 10 mL, ThermoFisher). The released cells were collected by centrifugation at 1000 rpm at 4 °C for 5 min. The collected cell pellet was washed once with cold DPBS (2 mL) and lysed by incubation with lysis buffer (150–300  $\mu$ L, 50 mM Tris pH 7.5, 150 mM NaCl, 0.5% Triton X-100, and 10% glycerol) at 4 °C for 20 min with gentle rocking. The cell debris was removed by spinning at 13,200 rpm for 20 min at 4 °C. The protein concentration in the soluble fraction was

determined by a Bradford assay (Biorad). The lysates were either used immediately or stored at  $-80^{\circ}\text{C}$  for future use.

**Assessment of PPP1R12A Knockdown and GADD34 Expression.** L6 lysates (160  $\mu\text{g}$  total protein for the PPP1R12A knockdown studies; 100  $\mu\text{g}$  total protein for the GADD34 expression studies) from Dox-treated and untreated cells were separated by a 10% SDS-PAGE after boiling at  $95^{\circ}\text{C}$  for 1 min in a Laemmli sample buffer (60 mM Tris-HCl pH 6.8, 2% SDS, 10% glycerol, 0.0005% bromophenol blue, and 2% beta-mercaptoethanol). Proteins were transferred onto a membrane (Millipore, Immobilon P), and the levels of PPP1R12A and GADD34 were assessed by western blotting using primary antibodies to PPP1R12A (Santa Cruz Biotechnology: sc-25618) and GADD34 (Santa Cruz Biotechnology: sc-46661). Total proteins were visualized by Sypro Ruby gel staining (Invitrogen) using a Typhoon imager (GE Healthcare Life Sciences).<sup>24</sup>

**Kinase-Catalyzed Biotinylation to Identify Phosphatase Substrates (K-BIPS) Experiment.** L6 lysates (600  $\mu\text{g}$  total protein) with and without Dox treatment were biotin labeled by incubation with ATP-biotin (2 mM) for 2 h at  $31^{\circ}\text{C}$  in a final volume of 32  $\mu\text{L}$ . After removing a portion of lysates (100  $\mu\text{g}$ ) for future analysis as the input, the rest of the lysates were filtered using centrifugal filter columns (Millipore, 3 kDa cutoff) to remove the remaining ATP-biotin and cellular biotin. Streptavidin resin (250  $\mu\text{L}$ , Genscript) was washed three times with binding buffer (200–250  $\mu\text{L}$ ; 0.1 M phosphate pH 7.2, 0.15 M NaCl). Samples were incubated with the washed streptavidin resin for 1 h at room temperature with rotation in spin columns (ThermoFisher). The flow-through was collected by centrifugation at 2300 rpm at room temperature for 1 min. Streptavidin beads were then washed 10 times with binding buffer (200–250  $\mu\text{L}$ ) and 4 times with water (200–250  $\mu\text{L}$ ). The final wash was saved to be later analyzed. Bound proteins were eluted by boiling the beads in 2% SDS in water (250  $\mu\text{L}$ ) for 8 min. The eluted protein sample was dried by lyophilization. The dried eluate was resuspended in water ( $\sim 30$   $\mu\text{L}$ ). The input, flow-through, last wash, and eluate were run on a 10% SDS-PAGE gel after boiling at  $95^{\circ}\text{C}$  for 1 min in the Laemmli sample buffer. Total proteins were visualized by Sypro Ruby stain (Invitrogen). The proteins in eluate lanes were in-gel digested, as previously described.<sup>30</sup> Digested peptides were analyzed on a Q-Exactive mass spectrometer (Thermo) after being separated by an EASY nLC-1000 UHPLC system (Thermo) under acidic conditions (0.1% formic acid). MS1 profiling used a 375–1600  $m/z$  range at a resolution of 70,000. MS2 fragmentation was achieved with higher energy collision-induced dissociation (HCD) of the top 15 ions using a 1.6  $m/z$  window and normalized collision energy of 29. Dynamic exclusion was used (15 s). The mass spectrometry proteomics data have been deposited to the ProteomeXchange Consortium via the PRIDE<sup>31</sup> partner repository with the data set identifiers PXD035211 and 10.6019/PXD035211, PXD035212 and 10.6019/PXD035212, and PXD035213 and 10.6019/PXD035213, which correspond to each trial of the data.

**MS Data Analysis.** MaxQuant (version 1.5.2.8)<sup>32,33</sup> was used with a rat database downloaded from Uniprot. Oxidation of methionine and acetylation of protein N-termini were set as variable modifications. The iodoacetamide derivative of cysteine was defined as a fixed modification. Searches included two missed tryptic cleavages. Mass tolerances for parent ions were 20 ppm for the first search, 4.5 ppm for the second

search, and 20 ppm for fragment ions. Minimum protein and peptide identification probabilities were used at  $\leq 1\%$  false discovery rate (FDR) as determined by a reversed database search. All other parameters were default settings (Table S1A). To generate a K-BIPS hit list of PP1c-PPP1R12A candidate substrates, proteins that showed at least 1.1-fold enrichment in untreated (PPP1R12A present) compared to Dox-treated (PPP1R12A knockdown) samples' reproducibility in all three biological replicates were identified (Table S1B). To create a high confidence list of substrate hits, the Student paired  $t$  test with a two-tailed distribution was used to identify candidate substrates showing low variability in the label-free quantitation intensity values via a  $p$  value  $< 0.05$ , in addition to a 1.1-fold enrichment in all three biological replicates (Table 1 and Table S1C).

**Table 1. High Confidence Protein Hits Identified by K-BIPS<sup>a</sup>**

gene ID	gene name	$p$ value	interaction	function
D4ABY2	COPG2	0.00303		protein transport
Q68FS2	COPS4	0.00477		signalosome complex
P13233	CN37	0.00510	PPP1CA	RNA metabolism
Q9JLJ3	AL9A1	0.01457		polyamine biosynthesis
Q66H94	FKBP9	0.01553		protein folding
P47196	AKT1	0.01837	PPP1CA/B/C	<b>cytoskeletal rearrangement<sup>49</sup></b>
Q5XI81	FXR1	0.01873		<b>cell migration<sup>50</sup></b>
Q63081	PDIA6	0.02147		unfolded protein response
P10860	DHE3	0.02728		TCA cycle
Q5M7U6	ARP2	0.02793	PPP1CB, PPP1R12A	<b>actin polymerization<sup>51</sup></b>
P21531	RL3	0.02851	PPP1CC	ribonucleoprotein complex
P97546	NPTN	0.03119		<b>cell adhesion<sup>52</sup></b>
P11598	PDIA3	0.03818		protein folding
O70199	UGDH	0.04894		nucleotide biosynthesis

<sup>a</sup>Candidate hits show an average enrichment of at least 1.4-fold and high significance using the paired Student  $t$  test with two-tailed distribution ( $p < 0.05$ , Table S1C). Interaction information was obtained from the BioGrid database. Known functional roles of the identified proteins were obtained from the Uniprot database, with hits showing functions similar to those of PP1c-PPP1R12A bolded and reference provided. PPP1CA, PPP1CB, and PPP1CC refer to the  $\alpha$ ,  $\beta$ , and  $\gamma$  catalytic subunits of PP1, respectively.

Protein classifications (cellular compartment, biological process, and molecular function) were analyzed using the DAVID Bioinformatics Resources 6.8 software (<https://david.ncifcrf.gov/>),<sup>34,35</sup> with the data plotted in Microsoft Excel (Figure 2). Abundance analysis was performed using the PAXdb database ([pax-db.org](http://pax-db.org)) and the integrated *Rattus Norvegicus* database,<sup>36</sup> with the data plotted in Microsoft Excel (Figure S3). The known physical protein–protein interactions among the hit proteins in human cells were mapped using the GeneMANIA 3.4.0 application in Cytoscape 3.3.0.<sup>37–40</sup> Analysis of common protein hits compared to prior trapping was performed using Canva ([www.canva.com/graphs/venn-diagrams/](http://www.canva.com/graphs/venn-diagrams/)).

**AKT1 and COPS4 Confirmation Using K-BIPS.** L6 lysates treated with and without Dox (600  $\mu\text{g}$  total protein)

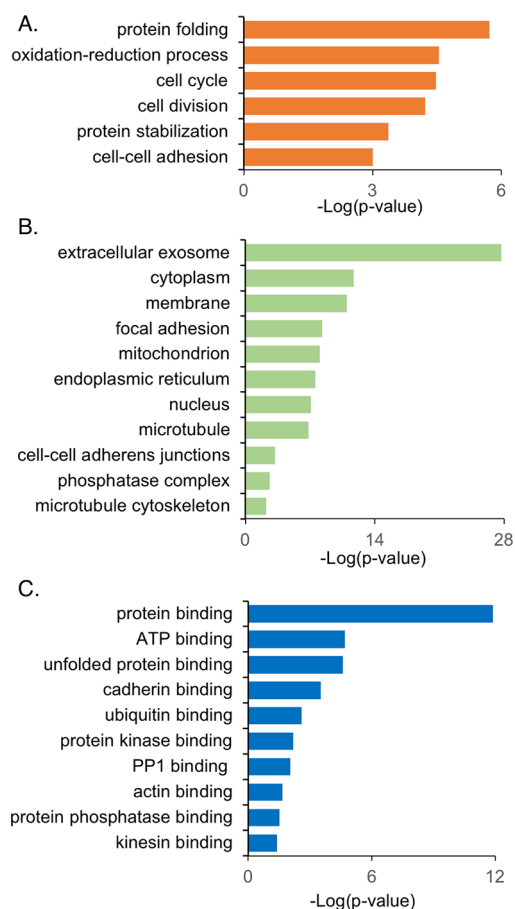


**Figure 2.** Functional classification of candidate PP1c-PPP1R12A substrates. The 136 proteins identified from substrate trapping (Table S1B) were classified according to biological processes (A), cellular localization (B), and molecular function (C) using the DAVID 6.8 software.<sup>34,35</sup>

were biotinylated and streptavidin enriched as described above. The enriched proteins were separated on a 10% SDS-PAGE, along with the input and the final wash, to assess protein enrichment. The proteins were then transferred onto a PVDF membrane (Millipore Immobilon-P) and probed with specific antibodies for AKT1 (Cell Signaling: 2938S) and COPS4 (Bethyl Laboratories: A300-013A).

**AKT1 and COPS4 Validation Using Phos-tag SDS-PAGE.** Proteins in lysates from untreated or Dox-treated L6 cells (100  $\mu$ g total protein) were separated using 10% SDS-PAGE and 10% SDS-PAGE containing the Phos-tag reagent (25  $\mu$ M, Fujifilm Wako Chemicals U.S.A. Corporation) and  $ZnCl_2$  (10  $\mu$ M). Total protein levels were assessed with Sypro Ruby gel stain (Invitrogen) and visualized using a Typhoon imager (GE Healthcare Life Sciences). Proteins in the gels were electrotransferred to a PVDF membrane (Millipore Immobilon-P), and AKT1, COPS4, and PPP1R12A protein levels were visualized with AKT1 (Cell Signaling: 2938S), COPS4 (Bethyl Laboratories: A300-013A), and PPP1R12A (Santa Cruz Biotechnology: sc-25618) primary antibodies using a Typhoon imager (GE Healthcare Life Sciences).

## RESULTS

To identify PP1c-PPP1R12A substrates with K-BIPS, we initially generated PPP1R12A-knockdown lysates. The L6 skeletal muscle cell line containing a Dox-inducible PPP1R12A

shRNA expression cassette was grown in the presence or absence of Dox, as reported,<sup>23</sup> with knockdown confirmed using gel analysis. Reduced PPP1R12A levels were observed in Dox-treated lysates (Figure S1, lane 2) compared to untreated lysates (Figure S1, lane 1), confirming successful knockdown.

**K-BIPS with PPP1R12A Knockdown.** To perform K-BIPS using the PPP1R12A knockdown conditions (Figure 1B–E and Figure S2A), ATP-biotin was incubated with untreated and Dox-treated lysates to biotinylate phosphoproteins. Biotinylated proteins were then enriched using streptavidin resin from each sample, separated by SDS-PAGE (Figure S2B), and analyzed by LC–MS/MS after in-gel digestion. LC–MS/MS analysis identified a total of 1445 proteins among the three independent trials (Table S1A). Label-free quantitation using MaxQuant<sup>32,33</sup> was used to select for proteins enriched in untreated samples compared to the Dox-treated, PPP1R12A-knockdown samples in three independent trials. We found 136 proteins that were enriched in untreated samples compared to Dox-treated samples by at least 1.1-fold in all three independent trials (Table S1B).

The 136 proteins in the list were analyzed using DAVID Bioinformatics Resources 6.8 to categorize the protein hits according to biological processes, cellular localization, and molecular function (Figure 2).<sup>34,35</sup> As expected from the known biological processes of PPP1R12A, the list of possible candidates included proteins involved in cell division and cell–cell adhesion (Figure 2A). Likewise, candidate substrates were localized in focal adhesions, microtubules, cell–cell adherens junctions, and the microtubule cytoskeleton (Figure 2B), in addition to having functions in microtubule, kinesin, and actin binding (Figure 2C). Related to the role of PP1c-PPP1R12A in regulating phosphorylation, candidate proteins bound ATP, protein kinases, protein phosphatases, and PP1 (Figure 2C). A number of proteins involved in insulin signaling and the actin cytoskeleton were observed, including AKT1 (P47196), Profilin (PROF1, Pfn1, P62963), Nap125 (NP1L1, Q9Z2G8), and Arp2 (Actr2, Q5M7U6), which are consistent with the use of L6 skeletal muscle cells. Beyond the known functions of PP1c-PPP1R12A in skeletal muscle cells, proteins associated with cell cycle, oxidation–reduction processes, and protein stability were also observed (Figure 2A).

To complement the analysis of cellular functions and localization, the 136 candidate substrates were analyzed for known physical interactions in human cells using the GeneMania 3.4.0 application in Cytoscape 3.3.0 (Figure 3).<sup>37–40</sup> Among the 136 proteins, 12 proteins (Figure 3, blue) directly interact with PPP1R12A or the three catalytic subunits of PP1 (PP1CA/B/C, Figure 3, red). An additional 76 proteins interact with the PP1c-PPP1R12A complex indirectly through the direct interactors (Figure 3; green, orange, purple, and pink). This interactome analysis documents that 65% of hit proteins have known physical interactions with the PP1c-PPP1R12A complex, consistent with their proximity to the complex for dephosphorylation.

A key feature of K-BIPS is the incorporation of an enrichment step dependent on phosphatase activity prior to LC–MS/MS analysis, which is expected to isolate candidate substrates independent of protein abundances. To assess the dependence of protein abundance on K-BIPS enrichment, an analysis of the 136 proteins was also conducted using the Paxdb 4.1 protein abundance database (pax-db.org).<sup>36</sup> Among the 136 proteins, only 4 proteins were not represented in the databases (Q9QZR6, Q5XI81, Q6IRE4, Q5BJK8). The

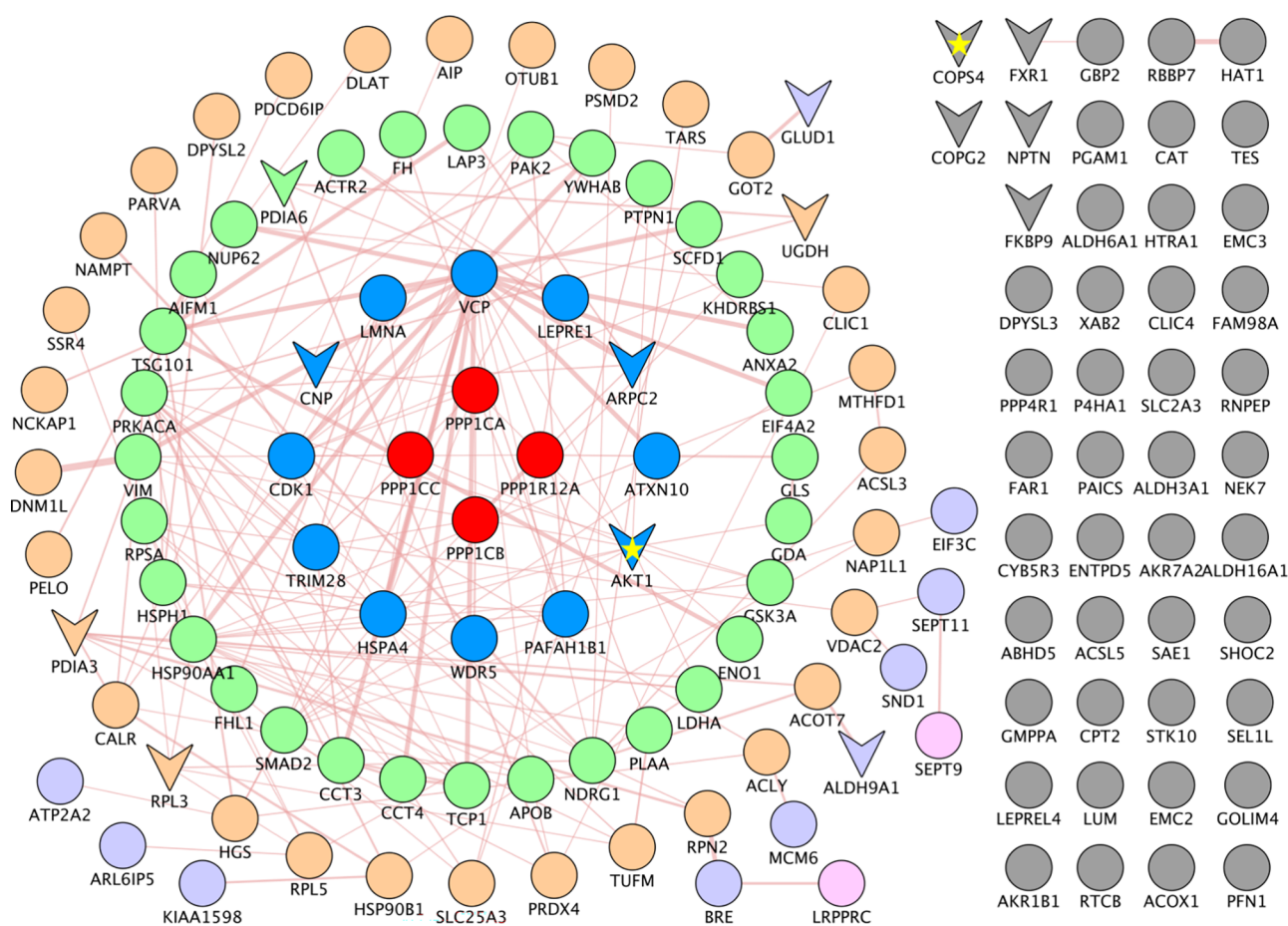


**Figure 3.** Interactome analysis of candidate PP1c-PPP1R12A substrates. The 136 proteins identified using K-BIPS were analyzed for evidence of physical interactions using the GeneMania 3.4.0 application in Cytoscape 3.3.0,<sup>37–40</sup> which mines databases including the BioGrid and iRefWeb, as well as primary literature. Colored shapes represent the degrees of interaction with PPP1R12A or the three catalytic subunits of PP1 (PPP1CA/B/C). Proteins encircling PP1c-PPP1R12A (red) are known direct interactors (blue), whereas the other proteins bind PP1c-PPP1R12A indirectly through one (green), two (orange), three (purple), or four (pink) associated proteins. The remaining proteins (gray) have no known interactions with the PP1c-PPP1R12A complex. Proteins with a V shape are identified in the highest confidence hit list after analysis using a Student *t* test (Table 1). The two starred high confidence proteins, AKT1 and COPS4, were further validated. Lines between proteins indicate a known physical interaction, with the thickness reflecting the confidence in the evidence for that interaction generated in GeneMania.

remaining 132 showed abundances ranging from 2269 ppm to 0.51 ppm (Figure S3) compared to the range of 21,179 ppm to 0.001 ppm for the integrated rat proteome in Paxdb (22,941 proteins, 74% coverage). The presence of both high- and low-abundance proteins in the hit list suggests that the enrichment by K-BIPS is independent of protein abundance.

In an earlier study that used the same L6 skeletal muscle cell line with inducible PPP1R12A knockdown, quantitative phosphoproteomics after metal ion affinity chromatography identified PP1c-PPP1R12A substrates.<sup>23</sup> Despite the use of insulin treatment, as well as TiO<sub>2</sub> enrichment of peptides instead of biotin enrichment of full-length proteins, one overlapping protein hit was observed between in the two data sets: NDRG1 (N-myc downstream-regulated gene 1 protein, Q6JE36). NDRG1 (NDR1/DRG1/Rit42/Cap43/RTP) is a phosphoprotein involved in hormone responses and cell growth, as well as cancers.<sup>41,42</sup> NDRG1 is dephosphorylated by PTEN and PTP $\alpha$  phosphatases,<sup>42,43</sup> although there is no prior relationship with PP1c-PPP1R12A.

Finally, to assess if K-BIPS differentiates substrates of the many phosphatase-regulatory subunit complexes in cells, we compared the results here with PP1c-PPP1R12A to our prior K-BIPS study with the PP1c-GADD24 complex under

conditions of the unfolded protein response (UPR). Among the 136 K-BIPS hits with the PP1c-PPP1R12A complex, only nine proteins were in common with the 130 K-BIPS hits of the PP1c-GADD24 complex under conditions of UPR (Figure S4), indicating a 3% overlap. In addition to these nine overlapping hits, COPS4 (CSN4) and CSN5 were found in the PP1c-PPP1R12A and PP1c-GADD24 K-BIPS studies, respectively, which both belong to the COP9 signalosome. The low level of overlap between the two studies suggests that K-BIPS identified proteins specific to each regulatory complex.

**High Confidence K-BIPS Hits and Validation.** To assess the value of the K-BIPS study, we next sought to identify high confidence hit proteins as candidates for validation experiments. To create a high confident hit list, a Student paired *t* test with two-tailed distribution was used to identify 14 hit proteins with 95% confidence among the original hit list (Table 1, Table S1C, and Figure 3). Four proteins from this high confidence list have known interactions with at least one of the three catalytic domains of PP1. Specifically, AKT1 has known interaction with all three catalytic subunits of PP1,<sup>44,45</sup> whereas CN37 (CNP), ARP2 (Actr2), and RL3 (RPL3) have known interaction with one catalytic subunit of PP1.<sup>46–48</sup> ARP2 is the only hit that interacts with PPP1R12A.<sup>47</sup> Beyond

known interactions, multiple high confidence hits play roles in cell adhesion and migration, consistent with the established role of PP1c in skeletal muscles (Table 1, bolded). AKT1 is involved in cytoskeletal rearrangement,<sup>49</sup> FXR1 is linked to cell migration,<sup>50</sup> ARP2 is connected to actin polymerization,<sup>51</sup> and NPTN is associated with cell adhesion.<sup>52</sup> These known interactions and functions of the high confidence high list suggest a role for PP1c in skeletal muscle cell functions.

Among the 14 high confidence hits, we selected AKT1 and COPS4 (also known as CSN4) for validation (Table 1). AKT1 interacts directly with all three PP1 catalytic subunits based on prior work and functions in cytoskeletal rearrangement,<sup>46–49</sup> making AKT1 a likely substrate. In contrast, COPS4 has no known interaction with the PP1c-PPP1R12A complex or known direct functions related to the PP1c-PPP1R12A complex, making COPS4 an unexpected substrate. Therefore, AKT1 and COPS4 represent two high confidence candidate substrates with different levels of prior evidence corroborating the K-BIPS discovery study.

K-BIPS was used with western blot analysis as a confirmation assay. Here, lysates from Dox-treated and untreated lysates were labeled with ATP-biotin, and biotinylated proteins were enriched using streptavidin resin. The purified proteins were then separated by SDS-PAGE, and the levels of enriched AKT1 and COPS4 were assessed by western blotting. The expectation for these studies is that Dox-treated samples would show reduced biotinylation of AKT1 and COPS4 due to PPP1R12A knockdown, loss of dephosphorylation, and inability to biotinylate already phosphorylated sites (Figure 1B–E). As expected based on the LC–MS/MS data, both AKT1 and COPS4 showed reduced biotin enrichment levels in Dox-treated lysates (Figure 4A,B, lane 2) compared to untreated lysates (Figure 4A,B, lane 1). As a control, the levels of AKT1 and COPS4 were equal in lysate input (Figure 4A,B, lanes 1 and 2), showing that the expressions of AKT1 and COPS4 were independent of PPP1R12A knockdown. The results confirmed the LC–MS/MS analysis by showing a similar PP1c-PPP1R12A-dependent biotinylation enrichment using gel methods.

To confirm that AKT1 and COPS4 are substrates of PP1c-PPP1R12A, Phos-tag SDS-PAGE was performed as a validation method. The Phos-tag additive interacts with phosphate groups to alter the migration of phosphorylated proteins, which can distinguish differentially phosphorylated protein bands. If PP1c-PPP1R12A influences the phosphorylation state of AKT1 or COPS4, additional bands after Phos-tag SDS-PAGE separation would be expected in the Dox-treated compared to untreated samples. Phos-tag SDS-PAGE was performed with proteins from untreated and Dox-treated L6 cell lysates followed by visualization of AKT1 and COPS4 by western blotting. As expected, two higher intensity bands of AKT1 were observed in Dox-treated knockdown compared to untreated samples (Figure 4C and Figure S7A). Quantification of both bands from three independent trials confirmed  $37 \pm 9$  and  $34 \pm 6\%$  reductions in band intensity in the untreated versus Dox-treated samples (Figure 4D and Figure S7C). The Phos-tag SDS-PAGE analysis is consistent with PP1c-PPP1R12A dephosphorylation of AKT1.

In contrast to AKT1, COPS4 was not validated as a PP1c-PPP1R12A substrate with Phos-tag SDS-PAGE. Despite confirmation of enrichment by K-BIPS using western blotting (Figure 4B), the Phos-tag data did not show elevated intensities of bands in the Dox-treated compared to untreated

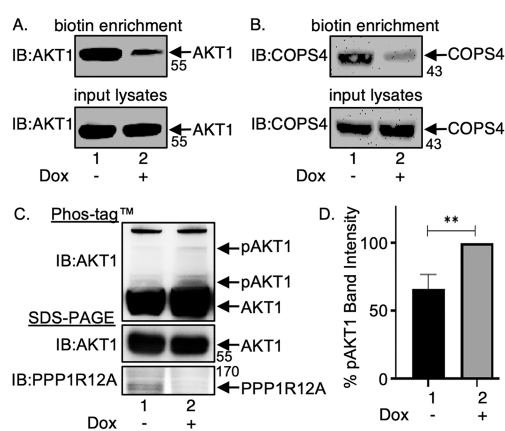


**Figure 4.** Validation of AKT1 and COPS4 as PP1c-PPP1R12A substrates. (A, B) L6 cells were treated with and without doxycycline (Dox) before cell lysis. Proteins in the lysates were labeled with ATP-biotin, and biotinylated proteins were enriched using streptavidin resin. Enriched biotinylated proteins in the eluates (top) and input lysates before enrichment (bottom) were separated by 10% SDS-PAGE (A and B). AKT1 (A) or COPS4 (B) levels were observed by immunoblotting (IB) using their respective antibodies. Additional independent trials are shown in Figures S5 and S6. (C) Proteins in the untreated and Dox-treated L6 cell lysates were separated using both Phos-tag SDS-PAGE and traditional SDS-PAGE. Proteins were transferred onto the PVDF membrane, and AKT1 and PPP1R12A were visualized using appropriate antibodies. Additional independent trials are shown Figure S7A. Molecular weight markers are indicated to the right of the gel images. (D) pAKT bands in the Figure 4C and Figure S7A were quantified using the ImageJ 1.52a software and normalized to the intensity in the Dox-treated sample (set to 100%, Figure S7B). A histogram of the mean and standard error from the bottom band was analyzed by the Student *t* test using GraphPad Prism 8.2.1 (\*\**p* = 0.006), with the top band analyzed in Figure S7C.

samples (Figure S8). The data imply that either COPS4 is not a direct substrate of PP1c-PPP1R12A or the Phos-tag SDS-PAGE analysis is not sensitive enough to monitor changes in phosphorylation as a function of PPP1R12A knockdown. As an alternative hypothesis, COPS5 was identified and validated as a substrate of the PP1-GADD34 phosphatase complex in our previous work.<sup>24</sup> Given that both COPS4 and COPS5 are subunits of the COP9 signalosome, we wondered if PPP1R12A knockdown could have possibly lowered the expression of GADD34, affected the COP9 signalosome, and changed the phosphorylation of COPS4, leading to a false negative result by LC–MS/MS. To test this alternative hypothesis, the effect of PPP1R12A knockdown on GADD34 expression was analyzed in untreated and Dox-treated L6 cell lysates. Equal GADD34 expression was observed in untreated and Dox-treated samples (Figure S9), which confirmed that there is no direct relationship between PPP1R12A and GADD34 subunits. Additional studies are needed to assess possible subtle changes in COPS4 phosphorylation due to the PP1c-PPP1R12A complex.

## DISCUSSION

Despite the involvement in human diseases, few substrates of PP1c-PPP1R12A are currently known and validated. To identify unanticipated PP1c-PPP1R12A substrates, we used a chemoproteomics method termed K-BIPS as a substrate discovery tool.<sup>24</sup> K-BIPS identified 136 putative PP1c-PPP1R12A substrates (Table S1B), with 14 high confidence

hits (Table 1 and Table S1C). Interestingly, four proteins from the high confidence K-BIPS hit list are interacting partners of PP1c subunits (Table 1). Additionally, several K-BIPS hits are associated with cell migration, cytoskeleton arrangement, actin polymerization, and cell division, consistent with known PPP1R12A functions (Table 1). Taken together, the data confirm that K-BIPS identified likely PP1c-PPP1R12A substrates.

Given the use of K-BIPS as a discovery method, secondary validation was needed to confirm the PP1c-PPP1R12A substrate relationship. Two putative substrates from the high confidence K-BIPS hit (Table 1 and Table S1C) were further studied, including the Ser/Thr kinase AKT1. K-BIPS with western blotting (Figure 4A) and Phos-tag SDS-PAGE (Figure 4C,D) confirmed that PP1c-PPP1R12A affects AKT1 phosphorylation. In addition to interacting with all three PP1 catalytic subunits (Table 1), AKT1 is implicated in cytoskeleton regulation during cell movement and adhesion,<sup>49</sup> similar to PPP1R12A. Consistent with our K-BIPS validation studies, prior work documented that AKT1 is dephosphorylated by the PP1 catalytic subunit *in vitro*.<sup>44</sup> However, prior work did not clarify which PP1 regulatory subunit is involved in dephosphorylation. The K-BIPS results suggest that the PP1c-PPP1R12A complex dephosphorylates AKT1, which might affect AKT1-dependent cytoskeleton arrangement. Interestingly, AKT1 silencing increases the inhibitory phosphorylation of PPP1R12A at T696.<sup>53</sup> Given that AKT1 silencing is known to affect PPP1R12A phosphorylation, the phosphorylation status of AKT1 might regulate PPP1R12A activity through a feedback mechanism.

The K-BIPS study identified the COP9 signalosome subunit COPS4 as a high confidence hit (Table 1 and Figure 4B). However, COPS4 was not validated as a PP1c-PPP1R12A substrate using Phos-tag SDS-PAGE (Figure S8) despite confirmation of enrichment by K-BIPS using western blotting (Figure 4B), which could be due to the low sensitivity of Phos-tag SDS-PAGE. Because COPS4 might be influenced by PP1c-PPP1R12A (Figure 3), although too subtly for detection by Phos-tag SDS-PAGE, we searched the literature for possible connections between COPS4, the COP9 signalosome, and PP1c-PPP1R12A. COPS4 has no known interaction with PP1c or PPP1R12A, although prior work documents that the COP9 signalosome affects PPP1R12A activity through the RhoA GTPase. In detail, GTP-bound RhoA activates the kinase activity of ROCK1, which then phosphorylates and inactivates PPP1R12A.<sup>54</sup> Further, RhoA levels in the cell are regulated through degradation by neddylation CUL3 ubiquitin ligase,<sup>55</sup> which is controlled by the COP9 signalosome.<sup>56</sup> The model that emerges is that the COP9 signalosome regulates PPP1R12A activities through RhoA/ROCK1-mediated phosphorylation. Consistent with the role of CUL3 and the COP9 signalosome in modulating RhoA and PPP1R12A biological functions, inhibition of either CUL3 or neddylation induced morphological changes in the cytoskeleton.<sup>55,57,58</sup> We also note that COPS1 (CSN1), COPS2 (CSN2), COPS3 (CSN3), and COPS8, which are other subunits of the signalosome complex, along with CUL3 and RhoA, were also observed in the K-BIPS proteomics data (Table S1B), although they were only enriched in two out of three biological replicates and did not satisfy the stringent criteria for K-BIPS hit selection. Nevertheless, the presence of multiple COP9 signalosome-associated proteins among the K-BIPS study and the discovery of COPS4 as a putative PP1c-PPP1R12A substrate suggest a feedback

mechanism where PPP1R12A activity is regulated to affect cytoskeleton arrangement through inhibitory phosphorylation and COP9 signalosome-mediated degradation. Our prior K-BIPS study with the PP1c-GADD34 complex identified another COP9 signalosome protein COPS5 as a substrate. Although the PP1c-GADD34 K-BIPS study was performed under conditions of the unfolded protein response (UPR), the two studies taken together suggest a role of various PP1c regulatory complexes in the COP9 signalosome.

The hormone leptin induces cell migration and invasion, with implications in cancer metastasis,<sup>59</sup> diabetic vasculopathy,<sup>60</sup> and angiogenesis.<sup>61</sup> Previous studies reported that leptin augments inhibitory phosphorylation of PPP1R12A through the activation of RhoA/ROCK pathway. Importantly, leptin-mediated cell migration and invasion were shown to depend on the activity of RhoA/ROCK pathway,<sup>59</sup> suggesting the involvement of PPP1R12A. Interestingly, the K-BIPS experiment isolated PDIA3 and DHE3 (GLUD1), two proteins sensitive to leptin. Leptin elevates the phosphorylation of PDIA3<sup>62,63</sup> while downregulating the expression of GLUD1.<sup>64</sup> The K-BIPS results imply that PPP1R12A mediates cell migration and invasion through regulation of PDIA3 and GLUD1. Given that leptin was not used in the current study, the results also suggest that PPP1R12A may employ PDIA3 and GLUD1 to respond to leptin-independent stimuli.

This study highlights the value of K-BIPS to discover and validate phosphatase substrates. One limitation of K-BIPS is the need to inactivate the Tyr phosphatase or Ser/Thr phosphatase-regulatory subunit of interest. Because of the lack of selective phosphatase inhibitors, particularly for Ser/Thr phosphatase-regulatory complexes, knockdown approaches, including the inducible knockdown used in this study, provide a reasonable alternative in chemical inhibition. Validation of phosphatase substrates after K-BIPS identification can be an additional challenge, particularly in cases where changes in phosphorylation are subtle or low stoichiometry and secondary gel-based methods lack sufficient sensitivity. In fact, the unsuccessful validation of COPS4 as a PP1c-PPP1R12A substrate using Phos-tag gel analysis exemplified this challenge. We show here that K-BIPS can also serve as a secondary validation method in cases where traditional gel-based methods are insufficient.

## CONCLUSIONS

K-BIPS uncovered multiple putative PP1c-PPP1R12A substrates, which further implicate PP1c-PPP1R12A activity in biological functions, such as cytoskeleton rearrangement, cell migration, adhesion, and cell division. Interestingly, the study identified PPP1R12A-regulating proteins as substrates, including the validated PPP1R12A kinase AKT1. Therefore, an unanticipated outcome of this K-BIPS study is evidence that PPP1R12A regulates itself through feedback mechanisms related to its substrates. Despite prior evidence linking PPP1R12A activity to important cellular functions, the molecular mechanisms whereby PPP1R12A exerts functional consequences are understudied. By discovering novel substrates, K-BIPS provides a valuable approach to gain insights into how PP1c-PPP1R12A mediates its diverse biological roles. With a known role of PPP1R12A in various disease states, the novel substrates of PP1c-PPP1R12A identified by K-BIPS will assist in the characterization of disease progression, with possible influence on the development of novel therapeutics to combat human diseases.

## ■ ASSOCIATED CONTENT

### SI Supporting Information

The Supporting Information is available free of charge at <https://pubs.acs.org/doi/10.1021/acsomega.3c01944>.

PPP1R12A knock down in L6 cells (Figure S1); gel images of K-BIPS experiments used for LC–MS/MS analysis (Figure S2); abundance analysis of candidate substrates from the PP1c-PPP1R12A K-BIPS study (Figure S3); comparison of the two PP1c K-BIPS studies (Figure S4); validation of AKT1 as a PP1c-PPP1R12A substrate using K-BIPS (Figure S5); validation of COPS4 as a PP1c-PPP1R12A substrate using K-BIPS (Figure S6); AKT1 validation as a PP1c-PPP1R12A substrate using Phos-tag SDS (Figure S7); COPS4 validation as a PP1c-PPP1R12A substrate using Phos-tag SDS (Figure S8); PPP1R12A and GADD34 expression after Dox treatment (Figure S9); LC–MS/MS data are available via ProteomeXchange with identifiers PXD035211, PXD035212, and PXD035213 (PDF)

All LC–MS/MS data (Table S1) (XLSX)

## ■ AUTHOR INFORMATION

### Corresponding Author

Mary Kay H. Pflum – Department of Chemistry, Wayne State University, Detroit 48202-3489 Michigan, United States; Email: [pflum@chem.wayne.edu](mailto:pflum@chem.wayne.edu)

### Authors

Pavithra M. Dedigama-Arachchige – Department of Chemistry, Wayne State University, Detroit 48202-3489 Michigan, United States

Nuwan P.N. Acharige – Department of Chemistry, Wayne State University, Detroit 48202-3489 Michigan, United States

Xiangmin Zhang – Department of Pharmaceutical Sciences, Wayne State University, Detroit 48201 Michigan, United States

Hannah J. Bremer – Department of Chemistry, Wayne State University, Detroit 48202-3489 Michigan, United States

Zhengping Yi – Department of Pharmaceutical Sciences, Wayne State University, Detroit 48201 Michigan, United States

Complete contact information is available at:

<https://pubs.acs.org/doi/10.1021/acsomega.3c01944>

### Author Contributions

P.M.D. performed all experiments except the Phos-tag SDS-PAGE study (Figure 4C,D and Figures S7 and S8) and the Gadd34 expression level study (Figure S9) that were performed by N.P.N.A. X.Z. and Z.Y. generated the PPP1R12A knockdown L6 muscle cells. M.K.H.P. conceived the project. M.K.H.P., P.M.D., and Z.Y. carried out experimental design and interpretation. P.M.D., X.Y., H.J.B., Z.Y., and M.K.H.P. wrote the manuscript. All authors have given approval to the final version of the manuscript.

### Notes

The authors declare no competing financial interest.

## ■ ACKNOWLEDGMENTS

We would like to thank the National Institutes of Health (GM079529 and GM131821: Pflum; DK107666: Yi) and

Wayne State University for funding; the Wayne State University and Karmanos Cancer Center Proteomics Core, which is supported by NIH Grants P30 ES020957, P30 CA022453, and S10 OD010700; J. Caruso and N. Carruthers for technical support; and R. Beltman, A. Gamage, C. Gary, and V. Ramanayake-Mudiyansele for comments on the manuscript. The content is solely the responsibility of the authors and does not necessarily represent the official views of the National Institutes of Health.

## ■ REFERENCES

- (1) Graves, J. D.; Krebs, E. G. Protein phosphorylation and signal transduction. *Pharmacol. Ther.* **1999**, *82*, 111–121.
- (2) Hunter, T. Protein kinases and phosphatases: the yin and yang of protein phosphorylation and signaling. *Cell* **1995**, *80*, 225–236.
- (3) Adams, J. A. Kinetic and Catalytic Mechanisms of Protein Kinases. *Chem. Rev.* **2001**, *101*, 2271–2290.
- (4) Roskoski, R., Jr. Properties of FDA-approved small molecule protein kinase inhibitors. *Pharmacol. Res.* **2019**, *144*, 19–50.
- (5) Jackson, M. D.; Denu, J. M. Molecular reactions of protein phosphatases—insights from structure and chemistry. *Chem. Rev.* **2001**, *101*, 2313–2340.
- (6) Soulsby, M.; Bennett, A. M. Physiological signaling specificity by protein tyrosine phosphatases. *Physiology* **2009**, *24*, 281–289.
- (7) Andersen, J. N.; Mortensen, O. H.; Peters, G. H.; Drake, P. G.; Iversen, L. F.; Olsen, O. H.; Jansen, P. G.; Amderesen, H. S.; Tonks, N. K.; Moller, N. P. Structural and evolutionary relationships among protein tyrosine phosphatase domains. *Mol. Cell. Biol.* **2001**, *21*, 7117–7136.
- (8) Shi, Y. Serine/threonine phosphatases: mechanism through structure. *Cell* **2009**, *139*, 468–484.
- (9) Ceulemans, H.; Bollen, M. Functional diversity of protein phosphatase-1, a cellular economizer and reset button. *Physiol Rev* **2004**, *84*, 1–39.
- (10) Bollen, M.; Peti, W.; Ragusa, M. J.; Beullens, M. The extended PP1 toolkit: designed to create specificity. *Trends Biochem. Sci.* **2010**, *35*, 450–458.
- (11) Piheiro, A. S.; Marsh, J. A.; Forman-Kay, J. D.; Peti, W. Structural signature of the MYPT1-PP1 interaction. *J. Am. Chem. Soc.* **2011**, *133*, 73–80.
- (12) Martinez-Lemus, L. A.; Hill, M. A.; Meininger, G. A. The plastic nature of the vascular wall: a continuum of remodeling events contributing to control of arteriolar diameter and structure. *Physiology* **2009**, *24*, 45–57.
- (13) Serrano, L.; McDonald, P. C.; Lock, F.; Muller, W. J.; Dedhar, S. Inactivation of the Hippo tumour suppressor pathway by integrin-linked kinase. *Nat. Commun.* **2013**, *4*, 2976.
- (14) Kiss, A.; Lontay, B.; Becsi, B.; Markasz, L.; Olah, E.; Gergely, P.; Erdodi, F. Myosin phosphatase interacts with and dephosphorylates the retinoblastoma protein in THP-1 leukemic cells: its inhibition is involved in the attenuation of daunorubicin-induced cell death by calyculin-A. *Cell Signal* **2008**, *20*, 2059–2070.
- (15) Yamashiro, S.; Yamakita, Y.; Totsukawa, G.; Goto, H.; Kaibuchi, K.; Ito, M.; Hartshorne, D. J.; Matsumura, F. Myosin phosphatase-targeting subunit 1 regulates mitosis by antagonizing polo-like kinase 1. *Dev. Cell* **2008**, *14*, 787–797.
- (16) Xia, D.; Stull, J. T.; Kamm, K. E. Myosin phosphatase targeting subunit 1 affects cell migration by regulating myosin phosphorylation and actin assembly. *Exp. Cell Res.* **2005**, *304*, 506–517.
- (17) Matsumura, F.; Hartshorne, D. J. Myosin phosphatase target subunit: Many roles in cell function. *Biochem. Biophys. Res. Commun.* **2008**, *369*, 149–156.
- (18) Eto, M.; Kirkbride, J. A.; Brautigan, D. L. Assembly of MYPT1 with protein phosphatase-1 in fibroblasts redirects localization and reorganizes the actin cytoskeleton. *Cell Motil Cytoskeleton* **2005**, *62*, 100–109.
- (19) Birukova, A. A.; Smurova, K.; Birukov, K. G.; Usatyuk, P.; Liu, F.; Kaibuchi, K.; Ricks-Cord, A.; Natarajan, V.; Alieva, I.; Garcia, J. G.;

Verin, A. D. Microtubule disassembly induces cytoskeletal remodeling and lung vascular barrier dysfunction: role of Rho-dependent mechanisms. *J. Cell. Physiol.* **2004**, *201*, 55–70.

(20) Li, J.; Liu, X.; Liao, J.; Tian, J.; Wang, J.; Wang, X.; Zhang, J.; Xu, X. MYPT1 sustains centromeric cohesion and the spindle-assembly checkpoint. *J. Genet. Genomics* **2013**, *40*, 575–578.

(21) Geetha, T.; Langlais, P.; Luo, M.; Mapes, R.; Lefort, N.; Chen, S. C.; Mandarino, L. J.; Yi, Z. Label-free proteomic identification of endogenous, insulin-stimulated interaction partners of insulin receptor substrate-1. *J. Am. Soc. Mass Spectrom.* **2011**, *22*, 457–466.

(22) Chao, A.; Zhang, X.; Ma, D.; Langlais, P.; Luo, M.; Mandarino, L. J.; Zingsheim, M.; Pham, K.; Dillon, J.; Yi, Z. Site-specific phosphorylation of protein phosphatase 1 regulatory subunit 12A stimulated or suppressed by insulin. *J. Proteomics* **2012**, *75*, 3342–3350.

(23) Zhang, X.; Ma, D.; Caruso, M.; Lewis, M.; Qi, Y.; Yi, Z. Quantitative phosphoproteomics reveals novel phosphorylation events in insulin signaling regulated by protein phosphatase 1 regulatory subunit 12A. *J. Proteomics* **2014**, *109*, 63–75.

(24) Dedigama-Arachchige, P. M.; Acharige, N. P. N.; Pflum, M. K. H. Identification of PP1-Gadd34 substrates involved in the unfolded protein response using K-BIPS, a method for phosphatase substrate identification. *Mol. Omics* **2018**, *14*, 121–133.

(25) Green, K. D.; Pflum, M. K. H. Kinase-catalyzed biotinylation for phosphoprotein detection. *J. Am. Chem. Soc.* **2007**, *129*, 10–11.

(26) Senevirathne, C.; Embogama, D. M.; Anthony, T. A.; Fouda, A. E.; Pflum, M. K. The generality of kinase-catalyzed biotinylation. *Bioorg. Med. Chem.* **2016**, *24*, 12–19.

(27) Dedigama-Arachchige, P. M.; Pflum, M. K. K-CLASP: A Tool to Identify Phosphosite Specific Kinases and Interacting Proteins. *ACS Chem. Biol.* **2016**, *11*, 3251–3255.

(28) Senevirathne, C.; Pflum, M. K. Biotinylated phosphoproteins from kinase-catalyzed biotinylation are stable to phosphatases: implications for phosphoproteomics. *ChemBioChem* **2013**, *14*, 381–387.

(29) Acharige, N. P. N.; Pflum, M. K. H. L-Lactate Dehydrogenase Identified as a Protein Tyrosine Phosphatase 1B Substrate by Using K-BIPS. *ChemBioChem* **2021**, *22*, 186–192.

(30) Shevchenko, A.; Tomas, H.; Havlis, J.; Olsen, J. V.; Mann, M. In-gel digestion for mass spectrometric characterization of proteins and proteomes. *Nat. Protoc.* **2006**, *1*, 2856–2860.

(31) Perez-Riverol, Y.; Bai, J.; Bandla, C.; Garcia-Seisdedos, D.; Hewapathirana, S.; Kamatchinathan, S.; Kundu, D. J.; Prakash, A.; Frericks-Zipper, A.; Eisenacher, M.; Walzer, M.; Wang, S.; Brazma, A.; Vrcaino, J. A. The PRIDE database resources in 2022: a hub for mass spectrometry-based proteomics evidences. *Nucleic Acids Res.* **2022**, *50*, D543–D552.

(32) Cox, J.; Mann, M. MaxQuant enables high peptide identification rates, individualized p.p.b.-range mass accuracies and proteome-wide protein quantification. *Nat. Biotechnol.*, *26* ( ), 1367–1372.

(33) Tyanova, S.; Temu, T.; Carlson, A.; Sinitcyn, P.; Mann, M.; Cox, J. Visualization of LC-MS/MS proteomics data in MaxQuant. *Proteomics* **2015**, *15*, 1453–1456.

(34) Huang, D. W.; Sherman, B. T.; Lempicki, R. A. Systematic and integrative analysis of large gene lists using DAVID bioinformatics resources. *Nat. Protoc.* **2009**, *4*, 44–57.

(35) Huang, D. W.; Sherman, B. T.; Lempicki, R. A. Bioinformatics enrichment tools: paths toward the comprehensive functional analysis of large gene lists. *Nucleic Acids Res.* **2009**, *37*, 1–13.

(36) Wang, M.; Herrmann, C. J.; Simonovic, M.; Szklarczyk, D.; von Mering, C. Version 4.0 of PaxDb: Protein abundance data, integrated across model organisms, tissues, and cell-lines. *Proteomics* **2015**, *15*, 3163–3168.

(37) Montojo, J.; Zuberi, K.; Rodriguez, H.; Kazi, F.; Wright, G.; Donaldson, S. L.; Morris, Q.; Bader, G. D. GeneMANIA Cytoscape plugin: fast gene function predictions on the desktop. *Bioinformatics* **2010**, *26*, 2927–2928.

(38) Warde-Farley, D.; Donaldson, S. L.; Comes, O.; Zuberi, K.; Badrawi, R.; Chao, P.; Franz, M.; Grouios, C.; Kazi, F.; Lopeez, C. T.; Maitland, A.; Mostafavi, S.; Montojo, J.; Shao, Q.; Wright, G.; Bader, G. D.; Morris, Q. The GeneMANIA prediction server: biological network integration for gene prioritization and predicting gene function. *Nucleic Acids Res.* **2010**, *38*, W214–W220.

(39) Cline, M. S.; Smoot, M.; Cerami, E.; Kuchinsky, A.; Landys, N.; Workman, C.; Christmas, R.; Avila-Campilo, I.; Creech, M.; Gross, B.; Hanspers, K.; Isserlin, R.; Kelley, R.; Killcoyne, S.; Lotai, S.; Maere, S.; Morris, J.; Ono, K.; Pavlovic, V.; Pico, A. R.; Vialaya, A.; Wang, P. L.; Adler, A.; Conklin, B. R.; Hood, L.; Kuiper, M.; Sander, C.; Schmulevich, I.; Schwikowski, B.; Warner, G. J.; Iderker, T.; Bader, G. D. Integration of biological networks and gene expression data using Cytoscape. *Nat. Protoc.* **2007**, *2*, 2366–2382.

(40) Shannon, P.; Markiel, A.; Ozier, O.; Baliga, N. S.; Wang, J. T.; Ramage, D.; Amin, N.; Schwikowski, B.; Ideker, T. Cytoscape: a software environment for integrated models of biomolecular interaction networks. *Genome Res.* **2003**, *13*, 2498–2504.

(41) Agarwala, K. L.; Kokame, K.; Kato, H.; Miyata, T. Phosphorylation of RTP, an ER stress-responsive cytoplasmic protein. *Biochem. Biophys. Res. Commun.* **2000**, *272*, 641–647.

(42) Park, K. C.; Menezes, S. V.; Kalinowski, D. S.; Sahni, S.; Jansson, P. J.; Kovacevic, Z.; Richardson, D. R. Identification of differential phosphorylation and sub-cellular localization of the metastasis suppressor, NDRG1. *Biochim Biophys Acta Mol Basis Dis* **2018**, *1864*, 2644–2663.

(43) Ly, P. T. T.; Stewart, C.; Pallen, C. J. PTP alpha is required for laminin-2-induced Fyn-Akt signaling to drive oligodendrocyte differentiation. *J. Cell Sci.* **2018**, *131*, jcs212076.

(44) Xiao, L.; Gong, L. L.; Yuan, D.; Deng, M.; Zeng, X. M.; Chen, L. L.; Zhang, L.; Yan, Q.; Lui, J. P.; Hu, X. H.; Sun, S. M.; Liu, J.; Ma, H. L.; Zheng, C. B.; Fu, H.; Chen, P. C.; Zhao, J. Q.; Xie, S. S.; Zou, L. J.; Xiao, Y. M.; Liu, W. B.; Zhang, J.; Liu, Y.; Li, D. W. Protein phosphatase-1 regulates Akt1 signal transduction pathway to control gene expression, cell survival and differentiation. *Cell Death Diff.* **2010**, *17*, 1448–1462.

(45) Flores-Delgado, G.; Liu, C. W.; Sposto, R.; Berndt, N. A limited screen for protein interactions reveals new roles for protein phosphatase 1 in cell cycle control and apoptosis. *J. Proteome Res.* **2007**, *6*, 1165–1175.

(46) Esteves, S. L.; Domingues, S. C.; da Cruz e Silva, O. A.; Fardilha, M.; da Cruz e Silva, E. F. Protein phosphatase 1alpha interacting proteins in the human brain. *OMICS* **2012**, *16*, 3–17.

(47) Hein, M. Y.; Hubner, N. C.; Poser, I.; Cox, J.; Nagaraj, N.; Toyoda, Y.; Gak, I. A.; Weisswange, I.; Mansfeld, J.; Buchholz, F.; Hyman, A. A.; Mann, M. A human interactome in three quantitative dimensions organized by stoichiometries and abundances. *Cell* **2015**, *163*, 712–723.

(48) Yadav, L.; Tamene, F.; Goos, H.; Van Drogen, A.; Katainen, R.; Aebersold, R.; Gstaiger, M.; Varjosalo, M. Systematic Analysis of Human Protein Phosphatase Interactions and Dynamics. *Cell Syst.* **2017**, *4*, 430–444.e5.

(49) Xue, G.; Hemmings, B. A. PKB/Akt-dependent regulation of cell motility. *J. Natl. Cancer Inst.* **2013**, *105*, 393–404.

(50) Le Tonqueze, O.; Kollu, S.; Lee, S.; Al-Salah, M.; Truesdell, S. S.; Vasudevan, S. Regulation of monocyte induced cell migration by the RNA binding protein, FXR1. *Cell Cycle* **2016**, *15*, 1874–1882.

(51) Welch, M. D.; DePace, A. H.; Verma, S.; Iwamatsu, A.; Mitchison, T. J. The human Arp2/3 complex is composed of evolutionarily conserved subunits and is localized to cellular regions of dynamic actin filament assembly. *J. Cell Biol.* **1997**, *138*, 375–384.

(52) Beesley, P. W.; Herrera-Molina, R.; Smalla, K. H.; Seidenbecher, C. The Neuroplastin adhesion molecules: key regulators of neuronal plasticity and synaptic function. *J. Neurochem.* **2014**, *131*, 268–283.

(53) Lee, J. H.; Ragolia, L. AKT phosphorylation is essential for insulin-induced relaxation of rat vascular smooth muscle cells. *Am J Physiol Cell Physiol* **2006**, *291*, C1355–C1365.

(54) Kimura, K.; Ito, M.; Amano, M.; Chihara, K.; Fukata, Y.; Nakafuku, M.; Yamamori, B.; Feng, J.; Nakano, T.; Okawa, K.; Iwamatsu, A.; Kaibuchi, K. Regulation of myosin phosphatase by Rho and Rho-associated kinase (Rho-kinase). *Science* **1996**, *273*, 245–248.

(55) Chen, Y.; Yang, Z.; Meng, M.; Zhao, Y.; Dong, N.; Yan, H.; Liu, L.; Ding, M.; Peng, H. B.; Shao, F. Cullin mediates degradation of RhoA through evolutionarily conserved BTB adaptors to control actin cytoskeleton structure and cell movement. *Mol. Cell* **2009**, *35*, 841–855.

(56) Wu, J. T.; Lin, H. C.; Hu, Y. C.; Chien, C. T. Neddylation and deneddylation regulate Cul1 and Cul3 protein accumulation. *Nat. Cell Biol.* **2005**, *7*, 1014–1020.

(57) Martin, D. S.; Wang, X. The COP9 signalosome and vascular function: intriguing possibilities? *Am. J. Cardiovasc. Dis.* **2015**, *5*, 33–52.

(58) Leck, Y. C.; Choo, Y. Y.; Tan, C. Y.; Smith, P. G.; Hagen, T. Biochemical and cellular effects of inhibiting Nedd8 conjugation. *Biochem. Biophys. Res. Commun.* **2010**, *398*, 588–593.

(59) Kato, S.; Abarzua-Catalan, L.; Trigo, C.; Delpiano, A.; Sanhueza, C.; Garcia, K.; Ibanez, C.; Hormazabal, K.; Diaz, D.; Branes, J.; Castellon, E.; Bravo, E.; Owen, G.; Cuello, M. A. Leptin stimulates migration and invasion and maintains cancer stem-like properties in ovarian cancer cells: an explanation for poor outcomes in obese women. *Oncotarget* **2015**, *6*, 21100–21119.

(60) Goetze, S.; Bungenstock, A.; Czupalla, C.; Eilers, F.; Stawowy, P.; Kintscher, U.; Spencer-Hansch, C.; Graf, K.; Nurnberg, B.; Law, R. E.; Fleck, E.; Grafe, M. Leptin induces endothelial cell migration through Akt, which is inhibited by PPARgamma-ligands. *Hypertension* **2002**, *40*, 748–754.

(61) Park, H. Y.; Kwon, H. M.; Lim, H. J.; Hong, B. K.; Lee, J. Y.; Park, B. E.; Jang, Y.; Cho, S. Y.; Kim, H. S. Potential role of leptin in angiogenesis: leptin induces endothelial cell proliferation and expression of matrix metalloproteinases in vivo and in vitro. *Exp. Mol. Med.* **2001**, *33*, 95–102.

(62) Kita, K.; Okumura, N.; Takao, T.; Watanabe, M.; Matsubara, T.; Nishimura, O.; Nagai, K. Evidence for phosphorylation of rat liver glucose-regulated protein 58, GRP58/ERp57/ER-60, induced by fasting and leptin. *FEBS Lett.* **2006**, *580*, 199–205.

(63) Bravo, S. B.; Caminos, J. E.; Gonzalez, C. R.; Vazquez, M. J.; Garces, M. F.; Cepeda, L. A.; Garcia-Rendueles, M. E.; Iglesias-Gamara, A.; Gomez-Diaz, C.; Lopez, M.; Castano, J. P.; Dieguez, C.; Nogueiras, R. Leptin and fasting regulate rat gastric glucose-regulated protein 58. *Int. J. Pept.* **2011**, *2011*, 969818.

(64) Nobet, J. N.; Goodwill, A. G.; Sassoon, D. J.; Kiel, A. M.; Tune, J. D. Leptin augments coronary vasoconstriction and smooth muscle proliferation via a Rho-kinase-dependent pathway. *Basic Res. Cardiol.* **2016**, *111*, 25.